Statistics and Its Interface Volume 10 (2017) 207–216

Box dimension estimation of multi-dimensional random fields via wavelet shrinkage

Ali Reza Taheriyoun and Yazhen Wang*

Computation of the box dimension for high-dimensional surfaces is much more complicated than the one-dimensional case. To obtain a fast computation, we employ the relationship between the box dimension and the wavelet coefficients of a surface through the local oscillation. This approach gives an appropriate consistent estimator of box dimension for noisy paths. The behavior of convergence is also studied under Hölder continuity assumption for the family of index-β Gaussian fields. We show that the precision of the estimation procedure is not affected by the growth of dimension of the sample path. We finally examine the properties of the proposed estimator using a simulation study and a real dataset on equlibration of a particular solution.

AMS 2000 subject classifications: Primary 60D65, 60G60; secondary 65T65.
Keywords and phrases: Box dimension, Hölder continuity, Index-β Gaussian field, Spatial adaptation, Wavelet.

1. INTRODUCTION

1.1 General aspect

Put a surface in an XYZ Cartesian system and consider XY plane as time index while Z represents the surface height in each index. We therefore analyze the surface as a noisy path of a random field. This idea would be extended similarly to higher dimensional real value data, which mainly appear in specially astronomical problems. Regardless of physics theories on the noise creation due to uncertainty, noise is an inseparable part of observations even in precise tools. We then often confront with noisy time plots which may cause misunderstanding in exploring the pattern of the surface. There are many spatial adaptation methods to approximate the model of smooth surfaces. On the other hand, for a rough surface, it would be very complicated to attribute a specific model to observation; therefore, it seems important to measure the lack of smoothness. The source of roughness in many surfaces is the stochastic fractal structure [24, Chapter 9] which makes it difficult to employ the simple Lebesgue measure and its derivatives such as dimension, length and cross-section. Particularly, the dimension of such surface is called fractal dimension. Different approaches to computing fractal dimension yield different criterion like Hausdorff and box dimension. The Hausdorff dimension is based on Hausdorff measure and box dimension uses simple variation with respect to the scale of gridding.

Box counting is one of the simplest methods of computing the erraticism [the phrase was coined by 1, Ch.8 to denote the measure of nervousness] of a graph or a set. Let A be a non-empty bounded subset in $\mathbb{R}^{N+1}$, $N \in \mathbb{N}$, and $\mathcal{C}_\delta(A)$ be the smallest number of sets of diameter lower than δ which cover A. Only for better imagination, and only here consider these sets as the grid boxes of side $\delta = M^{-j}$, where $M > 1$ and $j > 1$ are integer numbers. This means that at level j, only the cubes of side M^{-j} or greater are visible. As a characteristic of the erraticism, the box counting method suggests counting the minimum number of required boxes of side (or diameter) M^{-j} to cover A. Let $N_A(j)$ be the minimum number of such boxes. The scaling law indicates that $N_A(j)$ tends to infinity when $j \to \infty$; however, the power law precisely indicates an exponential relationship between the $N_A(j)$ and j. This fact was formally introduced by Mandelbrot [18] when he reexamined the observed data of [25] to show the effect of scale of a ruler in measuring the length of the coastlines of Britain. But, historically he mentioned that Richardson himself had pointed out this fact in 1920's. According to the linear relationship between $N_A(j)$ and $j \log M$, although the fraction $\log N_A(j)/(j \log M)$ varies by change of small values of j, it is expected to be fixed and equal to the slope of the linear relationship for large enough j's. Therefore, the erraticism of A can be measured through the limit behavior of slope by

$$\lim_{j\to\infty} \frac{\log N_A(j)}{j \log M}, \tag{1}$$

when the limit exists. Replacing the cubes with any arbitrary set of diameter δ brings forward the formal definition of the box dimension of A that is

$$\dim_{\mathrm{B}} A = \lim_{\delta\to 0} \frac{\log \mathcal{C}_\delta(A)}{-\log \delta}. \tag{2}$$

lim inf and lim sup are computed when the limit does not exist. The results are then called lower and upper box dimensions and denoted by $\overline{\dim}_{\mathrm{B}}$ and $\underline{\dim}_{\mathrm{B}}$, respectively. If the limit (2) exists the limit (1) will also exists [14]. It follows by (2) that $\dim_{\mathrm{B}} A \le N + 1$ and there is nothing to guar-

*Corresponding author. Yazhen Wang's research was partially supported by NSF grants DMS-105635, DMS-1265203 and DMS-1528375.

antee that the dimension remains an integer number. The definition of box dimension formulates the difficult concept of dimension using the simple geometric concept of minimal δ-cover without involving the effect of the induced measure of the random object. In the field of surface analysis, such simple and comprehensive definition has made it as one of the most interesting subjects to work on. In relative applied mathematical surveys, many other concepts (e.g. oscillation, Fourier coefficients and Hölder continuity) have been linked to the box dimension which return more useful versions of (2).

An intrinsic method in computing $\dim_{\mathrm{B}}$ for any set in $\mathbb{R}^{N+1}$ is covering the set by sub-cubes with volume $M^{-(N+1)}$. Therefore, the diameter of each sub-cube is $\sqrt{N+1}/M$ and tends to zero as $M \to \infty$. Thus, $\mathcal{C}_\delta$ is estimated by the number of sub-cubes and consequently the asymptotically unbiased estimator of $\dim_{\mathrm{B}}$ is $\log(\text{number of sub-cubes})/\log(\sqrt{N+1}/M)$. There are many other ways to construct sub-cubes and the question is what kind of gridding yields a better result? The discussion becomes more complicated when one is interested in the geometry of subsets in covering the set. For instance, one may apply the same procedure by using other sub-volumes than cubes. To the best of our knowledge, there is no familiar theoretical computation for the risks of estimators with respect to different covering methods. Thus, numerical study is the remaining approach for the comparison of estimators. Nevertheless, when the limit (2) exists, then $\dim_{\mathrm{H}} A \leq \dim_{\mathrm{B}} A$ where $\dim_{\mathrm{H}}$ is Hausdorff dimension. Thus, applying this inequality, it is possible to improve the risk of box dimension estimators by reseting the out-range values to the estimated Hausdorff dimension. Also, one may use an improved lower bound which was developed by [12].

There is a close direct relation between the number of elements of δ-cover of sets (here, assumed to be a path of a random field) and the variation of the path. On the other hand, one way to recognize the jumps and sudden changes in the values of a function is using wavelet coefficients [7], which is reviewed in Section 3. Linking the box dimension to wavelet coefficients is the basis of our estimator. This linkage was performed by Deliu and Jawerth [6] for real value functions on a bounded interval $I \subset \mathbb{R}$ [see 20, Chapter 6, for details]. The result is generalized here for real value functions on $\mathbf{I} \subset \mathbb{R}^N$ and then a consistent estimator grows up by applying an inferential solution to the ideal spatial adaptation problem. This procedure was introduced by Wang [30] for one-dimensional stochastic processes which is corrected and extended here.

A variety of approaches has been proposed for computing the box dimension of signals or surfaces. We refer to [2, Chapter 5] and [26] for an equivalent capacity based definition of fractal dimension which motivated the estimation of box dimension. A theoretic discussion on the computational algorithms for this kind of dimension was considered in [13]. Although the box dimension has been widely used in physics, engineering and geology, the statistical literatures containing theoretical approaches to accomplish good estimators are restricted and we mention [29] and [22] as essentially opening solutions for the statistical box dimension estimation. Statistical results such as asymptotic variance and bias of capacity based box dimension were motivated by Hall and Wood [11]. There is a collection of the fractal dimension estimation of one-dimensional stochastic processes and some extensions to higher moments in [10]. We also refer to [10] and all the references therein for a comprehensive literature review of the fractal estimation including an estimator based on the box counting method. The main problem in this collection is estimating the Hurst index and hence the Hausdorff dimension instead of box dimension. According to the inequality $N \leq \dim_{\mathrm{H}} A \leq \dim_{\mathrm{B}} A$, the variances of our method and the methods mentioned by [10] are not comparable. To the best of our knowledge, the box counting method has been employed only to estimate the Hölder or Hurst index in the literature of random fractal surfaces. The novelty of our method is estimating box dimension of surfaces directly and this a brand-new approach in multi-dimensional random fields.

1.2 Practical problem

Suppose that some small mass particles float in a fluid at a given thermodynamic temperature. The position of *a* mass have been formulated many times in physics theory and it has been traditionally referred to [9]. To analyze the motion equation of one particle, the path is usually considered as a realization of a three-dimensional Brownian motion. Thus, one may simply achieve the Hausdorff dimension of the Brownian motion (and generally the fractional Brownian motion) to compute the erraticism. For the case of more than one particle we intend to analyze a perspective motion of the whole suspension. This study is useful for some particular chemical reactions in such a way that the resulting product is collected as a sediment at the bottom of the container. At the beginning of the experiment, two liquid solutions are well shaken in a container and the nano-scale crystals of the final product are created as the result of the chemical reaction of the solutions. Passing the time, crystals connect to each other and constitute micro-scale crystals that are heavier and this phenomenon causes to the sedimentation of the product. In fact the particles of the product float in the liquid and the force of gravity yields to the sedimentation of particles. Obviously, the product is not extractable unless the suspension of the solid product and liquid container becomes stable with no movement of the solid particles. The aim of this study is introducing a method to determine the time of equilibrium in the suspension and hence the time of extraction of the product. To this end, we glint a thick light beam through the fluid and transfer the reflected beams to a transducer. We then have a perspective image in the apposite side of the glinted beam (see Figure 1). In fact, the positions of particles in a 3-dimensional Cartesian system

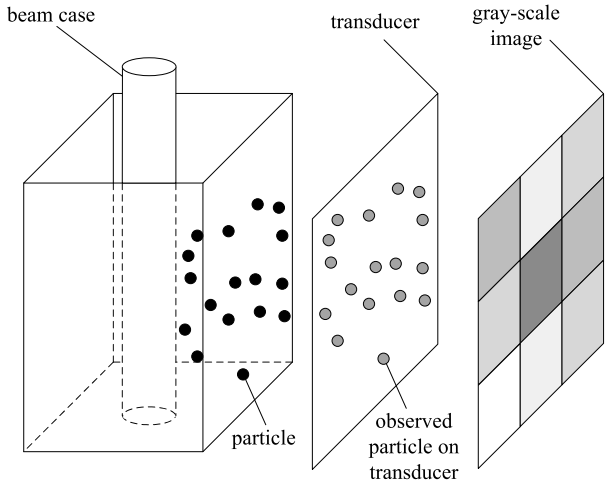

Figure 1. Observing the perspective of the whole particles.

is projected onto the 2-dimensional plane of the transducer. According to the large amount of the solid particles, the transducer will show a gray-scale image where the darkness of each pixel of this image indicates the density of solid points at the corresponding coordinate. After the stability, all the dark pixels gather at the bottom of image and therefore the mentioned gray-scale image is *almost* partitioned into a white and a black rectangle with a narrow unrecognizable border. A crucial problem in the product extraction is assessment of the true time of equilibrium and hence discharging the product. The larger width of the border states that the equilibrium is not achieved and we have to wait more. The irregularity of the particles motions in this border reflected to the gray-scale image and thus wide border (no equilibrium) produces an image with more erraticism. The box dimension estimation helps us to decide whether the equilibrium is acquired or not.

Returning to the problem of finding an appropriate model for the motions of crystals we look at the models suggested for the motion of a particle. The Brownian motion satisfies the Hölder continuity and then the first idea is to fit a random field satisfying the Hölder condition of a known order. This approach is not advisable since it brings forth a new parameter estimation problem. Meanwhile, under laboratory situations, the size of the image is worthwhile, and thus computing the intrinsic estimator of box dimension is time-consuming. Particularly, the computational procedure becomes considerably huge by examining the interaction between the irregularity of floated particles and the consumed time for equilibration of the heap in the fluid.

The outline of the paper will be organized as follows: In the following section we present the relationship between total oscillation and box dimension for multivariate functions. It also reviews the computation of box dimension using wavelet coefficients. A consistent estimator for noisy observations is introduced in Section 3. We also study the behavior of the estimator for random fields satisfying Hölder conditions in this section. The last section is devoted to a simulation study and a solution to the performed practical problem.

2. PRELIMINARIES

Let $X(\mathbf{t})$, $\mathbf{t} \in \mathbb{R}^N$, be an N-dimensional random field and let $x(\mathbf{t})$ be a realization of $X(\mathbf{t})$. Practically, the regular observations are collected through a bounded subset of $\mathbb{R}^N$, hence without loss of generality, assume that $\mathbf{t} \in \mathbf{I_0} = [0,1]^N$. At a resolution $\mathbf{j} = (j_1, \ldots, j_{N+1}) \in \mathbb{N}^{N+1}$ and translation $\mathbf{k} = (k_1, \ldots, k_N) \in \mathbb{N}^N$, let $Q_{\mathbf{j},\mathbf{k}}$ be a dyadic sub-cube of $\mathbf{I_0}$ i.e.

$$Q_{\mathbf{j},\mathbf{k}} = \Big\{ \mathbf{t} \in \mathbf{I_0} \Big| \frac{k_i}{M^{j_i}} \le t_i \le \frac{k_i+1}{M^{j_i}}; \\ i = 1, \ldots, N; k_i = 0, \ldots, M^{j_i} - 1 \Big\},$$

where M is an integer number greater than one. Since the resolution will be employed in covering the *graph* of random field, we let $\mathbf{j} \in \mathbb{N}^{N+1}$. To the best of our knowledge, almost all literatures used a special resolution $(j, \ldots, j)$, whereas in many practical problems, particularly in topographic maps, the resolution elements are different. Generally, there is no restriction to construct sub-cubes with equally scaled edge and one can replace M by M_i; however, following the procedures in Section 3.1, the results are the same. We also denote the oscillation of x over the set Q by

$$\operatorname{osc}(x; Q) = \sup_Q \{x(\mathbf{t}) - x(\mathbf{s}) | \mathbf{t}, \mathbf{s} \in Q\} = \sup_Q x - \inf_Q x.$$

Let $j_\cdot = \sum_{i=1}^N j_i$ and assume that, $\mathbf{I_0}$ is gridded by $N^{j_\cdot}$ numbers of the disjoint sub-cubes with the same volumes. Thus, the total oscillation of x over $\mathbf{I_0}$, with respect to the gridding constructed by $N^{j_\cdot}$ numbers of dyadic sub-cubes is defined by

$$\operatorname{Osc}(x; \mathbf{j}) = \sum_{\|Q\| = M^{-j_\cdot}} \operatorname{osc}(x; Q),$$

where the summation is over all dyadic sub-cubes Q with volume equal to $M^{-j_\cdot}$. Define $G_x(A) := \{(\mathbf{t}, x(\mathbf{t})) | \mathbf{t} \in A\}$ which is the graph of x on A. Kamont and Wolnik [16] showed that

$$\mathcal{C}_{M^{-j_\cdot}}\big(G_x(\mathbf{I_0})\big) \sim M^{j_\cdot} + M^{j_{N+1}} \operatorname{Osc}(x; \mathbf{j}),$$

where $A \sim B$ if $A = O(B)$ and $B = O(A)$. For the particular case $\mathbf{j} = (j, \ldots, j)$, the equivalence is changed to

$$\mathcal{C}_{M^{-Nj}}\big(G_x(\mathbf{I_0})\big) \sim M^{Nj} + M^j \operatorname{Osc}(x; j), \tag{3}$$

where the resolution $(j, \ldots, j)$ will be denoted in Osc and index of sub-cube Q by j for the sake of convenience. The remaining is the relationship between oscillation and wavelets which traces back to [6] where the oscillation of x is related

to the Besov space of particular index. The results were confronted by a counter-example by Kamont and Wolnik [16] and have been corrected by Jaffard [15].

Let $\mathcal{S}(\mathbb{R}^N)$ be the set of all $C^\infty(\mathbb{R}^N)$ functions whose derivatives are bounded when multiplied by any polynomial and $\mathcal{S}'(\mathbb{R}^N)$ be the linear space generated by the all continuous functionals in $\mathcal{S}(\mathbb{R}^N)$. Consider $\varphi \in \mathcal{S}(\mathbb{R}^N)$ with finite vanishing moments where support of the Fourier transform of φ is equal to $\{\mathbf{t} \in \mathbb{R}^N | 1/2 \le \|\mathbf{t}\| \le 2\}$. Then, for any function $x \in \mathcal{S}'(\mathbb{R}^N)$, there exists $\psi \in \mathcal{S}(\mathbb{R}^N)$ such that

$$x = \sum_{Q \in \mathcal{Q}} \langle x, \varphi_Q \rangle \psi_Q, \tag{4}$$

where $\varphi_{Q_{\mathbf{j},\mathbf{k}}}(\cdot) = 2^{j./2}\varphi(\mathbf{2^j}\cdot - \mathbf{k})$, $\mathbf{2^j} = (2^{j_1}, \ldots, 2^{j_N})$ and $\mathcal{Q}$ is the set of all dyadic sub-cubes $Q_{\mathbf{j},\mathbf{k}}$. The summation represents the wavelet decomposition of x, and φ is called mother wavelet or wavelet, briefly. The sequence $w_Q = \langle x, \varphi_Q \rangle$ is also called wavelet coefficient.

According to [15], the oscillation is linked to the wavelet by

$$\begin{aligned} &\liminf_{j\to\infty} \frac{\log \mathrm{Osc}(x,j)}{\log 2^{-j}} \\ &\quad = \limsup_{j\to\infty} \frac{\log \sum_{\mathbf{k}} \sup_{Q_{j',\mathbf{k}'}} |w_{Q_{j',\mathbf{k}'}}|}{j \log 2}. \end{aligned} \tag{5}$$

Employing (3) and (5) or directly from [15], for any continuous real value sample path x on $[0,1]^N$ we have

$$\begin{aligned} &\overline{\dim}_{\mathrm{B}} G_x([0,1]^N) \\ &\quad = \max\left\{N, 1 + \limsup_{j\to\infty} \frac{\log \sum_{\mathbf{k}} \sup_{Q_{j',\mathbf{k}'}} |w_{Q_{j',\mathbf{k}'}}|}{j \log 2}\right\}, \end{aligned} \tag{6}$$

with probability one. Also, replacing j by $\mathbf{j}$, the other version of this theorem is obtained. Thus, the equation (6) is changed to

$$\begin{aligned} &\overline{\dim}_{\mathrm{B}} G_x([0,1]^N) \\ &\quad = \max\left\{N, 1 + \limsup_{\mathbf{j}\to\boldsymbol{\infty}} \frac{\log \sum_{\mathbf{k}} \sup_{Q_{\mathbf{j}',\mathbf{k}'}} |w_{Q_{\mathbf{j}',\mathbf{k}'}}|}{\log 2^{j.}}\right\}, \end{aligned} \tag{7}$$

with probability one. Moreover, we may obtain (6) under Hölder continuity assumption instead of continuity. However, we apply this theorem only on continuous Gaussian fields where more details are discussed for index-β family in Section 4.

3. FRACTAL DIMENSION ESTIMATION

3.1 Consistent estimation

Suppose that y is a noisy path of the random field X. Thus, y could be decomposed into x, as a sample path of X, and a simple white noise. On the other hand, in many experimental samples from random fields, the sample path is observed on an N-dimensional lattice $\mathbb{L}$ with respect to a given resolution. Within each generated sub-cube in form of $(k_1/M^{j_1}, (k_1+1)/M^{j_1}) \times \ldots \times (k_N/M^{j_N}, (k_N+1)/M^{j_N})$, the linear approximation is applied due to the resolution restriction in data gathering. Figure 2 shows the linear approximation for $N = 2$. Therefore, our sample includes the values of x only on the nodes of the lattice $\mathbb{L}$ and there is no observation within sub-cubes.

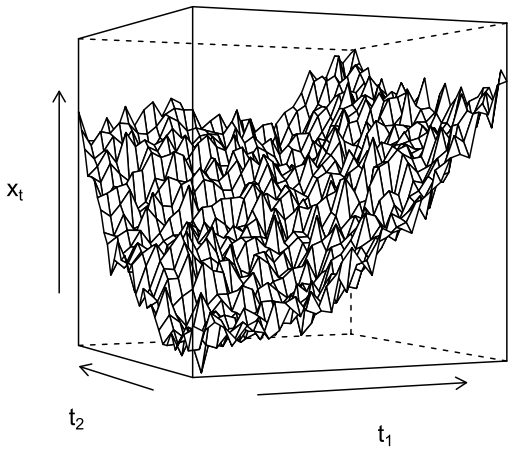

Figure 2. A noisy realization of X, using linear approximation within four neighboring nodes.

Since w_Q is essentially an integration using x, according to the sample path, there is no sufficient information to compute the exact wavelet coefficients. Using spatial adaptation, we may explore the empirical wavelet coefficients to employ (6). Let $\mathbf{n} = (n_1, \ldots, n_N)$ be the gridding level which means that the interval $[0,1]$ on the ith axis of the Cartesian system divided into $n_i = 2^{J_i+1}$ equidistant parts where $J_i > 1$ is an integer number. For convenience, let $\mathbf{l/n}$ denotes the node $(l_1/n_1, \ldots, l_N/n_N)$ for $0 \le l_i \le n_i$, $i = 1, \ldots, N$. The foregoing sampling assumptions confirms that the data $y(\mathbf{l/n})$ is observed from the nonparametric regression model

$$y\left(\frac{\mathbf{l}}{\mathbf{n}}\right) = x\left(\frac{\mathbf{l}}{\mathbf{n}}\right) + \varepsilon\left(\frac{\mathbf{l}}{\mathbf{n}}\right), \tag{8}$$

for $\mathbf{l/n} \in \mathbb{L}$ where $\varepsilon(\mathbf{l/n})$ are independently distributed as $N(0, \sigma^2)$ and x is the real path of X which we would like to find the wavelet coefficients for. In fact the normality is a mild assumption assumption in this nonparametric regression and we will see that eliminating this assumption does not harm the estimation procedure. A simple solution is recovering x by applying spatially adaption methods and let $\hat{x}$ denotes the recovered function. Then, compute the wavelet coefficients of $\hat{x}$ as an estimation of w. We employ the wavelet method to estimate the x function in this nonparametric regression. Simply speaking, the empirical wavelet coefficients of Y is computed using the observed surface, y, which is decomposed into the empirical wavelet coefficients of the parameter function, x, and the wavelet coefficients of the noise term. Considering the white noise

assumption, the wavelet coefficients of ε are identical and thus it suffices to remove it from the wavelet coefficients of y. To this end, thresholding the wavelet coefficients of y is suggested by Donoho and Johnstone [7]. Let w'_Q denotes the empirical wavelet coefficients of Y. A simple extension to higher dimension for an algorithm of discrete wavelet transformation of [17] has been explored in [21, Chapter 3]. Threshold w'_Q by a soft or hard thresholding rules according to the functions $\eta_S(w') = \text{sgn}(w')(|w'| - \lambda_{n_*})$ or $\eta_H(w') = |w'|1(|w'| > \lambda_{n_*})$, respectively where $n_* = \prod_{i=1}^N n_i$ is the sample size. Let us now reconstruct the function by the generated coefficients. This function estimation was introduced by Donoho and Johnstone [7] and was called Wavelet shrinkage. Employing the soft threshold by universal threshold $\lambda_{n_*} = \sigma(2\log n_*)^{1/2}$, returns the *VisuShrink* estimation which provides better visual features.

With reference to [7] and due to some restrictions for dyadic sub-cubes we have

$$w'_Q = w_Q + \frac{1}{\sqrt{n_*}} u_Q, \tag{9}$$

where u is the empirical wavelet coefficient of ε. For N-dimensional sample path on the gridding level $\mathbf{n}$, since the maximum resolution for ith element is $J_i = \log n_i - 1$, thus we denote the resolution by $\mathbf{j_n} = (j_{1n_1}, \ldots, j_{Nn_N})$.

Theorem 3.1. *Under the model (8) if y is a continuous noisy sample path of X on $[0,1]^N$, then*

$$\begin{aligned} T(y;\mathbf{j}_n) &= 1 + \frac{\log_2\left(\sum_{\mathbf{k}} \sup_{Q_{\mathbf{j}'_\mathbf{n},\mathbf{k}'}} |\eta_S(w'_{Q_{\mathbf{j}'_\mathbf{n},\mathbf{k}'}})|\right)}{j_{.\mathbf{n}}} \\ &\xrightarrow{p} \overline{\dim}_B G_X([0,1]^N), \end{aligned} \tag{10}$$

as $\mathbf{j_n} \to \boldsymbol{\infty}$ where $j_{.\mathbf{n}} = \sum_i j_{in_i}$.

A proof is given in Appendix A.

Employing (10), one may estimate the upper box dimension of the graph of a noisy random field, consistently. When the resolution and griding are the same in all directions of the Cartesian system, i.e. $\mathbf{n} = (n, \ldots, n)$ and $\mathbf{j_n} = (j_n, \ldots, j_n)$, the similar procedure can be performed by employing (6) to obtain

$$\begin{aligned} T(y;j_n) &= 1 + \frac{\log_2\left(\sum_{\mathbf{k}} |\sup_{Q_{j'_n,\mathbf{k}'}} \eta_S(w'_{Q_{j'_n,\mathbf{k}}})|\right)}{j_n} \\ &\xrightarrow{p} \overline{\dim}_B G_X([0,1]^N), \end{aligned}$$

as $j_n \to \infty$.

3.2 Diagnosis of the noise term

The normality assumption of the white noise plays a crucial role in achieving the minimaxity of the estimated function [see 8]. However, the lack of normality only targets the minimaxity and not the whole estimation procedure. There are plenty of empirical tests of normality in the literature of physics particularly for the Gaussianity tests of cosmic background waves [see 19, and the references therein]. However, the rejection area for the normality assumption in almost all of them are based practical experiences or they strongly require the stationarity assumption. To diagnose the assumptions of the noise term we first begin with the white noise assumption. Reconstruct $\hat{x}$ by applying the inverse wavelet transform on the thresholded empirical wavelet coefficients $\eta_S(w'_Q)$. Define the residual by $r(\mathbf{l/n}) = y(\mathbf{l/n}) - \hat{x}(\mathbf{l/n})$, for $\mathbf{l/n} \in \mathbb{L}$. A frequency domain approach could be useful in testing the white noise assumption. Set Λ as a discrete lattice obtained from gridding $[0, 2\pi]^N$ into n_* suitable nodes by dividing the ith edge into n_i parts. For a given constant v, define distinct points in Λ, D_v say, by $D_v = \{\boldsymbol{\lambda}_k; k = 1, \ldots, v\}$, where for any $j \neq k \leq v$ and any $\boldsymbol{\lambda}_j, \boldsymbol{\lambda}_k \in D_v$, $\boldsymbol{\lambda}_j$ is not equal to $\boldsymbol{\lambda}_k$ neither is it to $\mathbf{2\pi} - \boldsymbol{\lambda}_k$ where $\mathbf{2\pi}$ is an N-dimensional vector with elements equal to 2π. The N-dimensional periodogram of the residual process at the Fourier frequency $\boldsymbol{\lambda} \in D_v$ is defined as

$$I_r(\boldsymbol{\lambda};\mathbf{n}) = \frac{2}{n_*}\Big|\sum_{\mathbf{j=1}}^{\mathbf{n}} r(\frac{\mathbf{j}}{\mathbf{n}}) e^{\boldsymbol{\lambda}^T \cdot \frac{\mathbf{j}}{\mathbf{n}}}\Big|^2,$$

where $\boldsymbol{\lambda}^T$ is the transpose of $\boldsymbol{\lambda}^T$. Under some mild conditions [see 23, 27, for details], $\{I_r\boldsymbol{\lambda}\}_{\boldsymbol{\lambda}\in D_v}$ are asymptotically *iid* random variables from the exponential distribution. Thus, a rejection rule for the white noise assumption is defined by the rejection area of the hypothesis testing

$$H_0 : \{I_r\boldsymbol{\lambda}\}_{\boldsymbol{\lambda}\in D_v} \overset{iid}{\sim} \text{Exponential} \quad \text{versus} \quad H_1 : \text{not } H_0,$$

that is a simple goodness-of-fit test.

Once the white noise assumption is passed, under the normality assumption, the residuals are *iid* random variables from $N(0, \sigma^2)$. Thereupon, the normality is examined according to the testing problem of

$$H_0 : \{r(\mathbf{l/n})\}_{\mathbf{l/n}\in\mathbb{L}} \overset{iid}{\sim} \text{Normal} \quad \text{versus} \quad H_1 : \text{not } H_0,$$

where it is again a simple goodness-of-fit test.

3.3 Properties for index-β family

For an N-dimensional random field, let $E[X(\mathbf{t}+\mathbf{s}) - X(\mathbf{s})]^2$ be the incremental variance function. It is also called stationary incremental variance function when it does not change by $\mathbf{s}$ and is denoted by $\sigma^2(\mathbf{t})$. A zero-mean continuous Gaussian process with stationary increments belongs to index-β family if there exists $0 < \beta \leq 1$ such that

$$\beta = \sup\{\alpha | \sigma(\mathbf{t}) = o(\|\mathbf{t}\|^\alpha), \text{ as } \|\mathbf{t}\| \downarrow 0\}.$$

The index-β family satisfies the stochastic Hölder condition of order $\alpha < \beta$ which means that every sample path of X as an index-β family, satisfies

$$|x(\mathbf{t}+\mathbf{h}) - x(\mathbf{t})| \leq c\|\mathbf{h}\|^\alpha,$$

for every $\alpha < \beta$ where $c > 0$ is a constant [see 1, Chapter 8]. Therefore, the wavelet coefficients for $Q_{\mathbf{j},\mathbf{k}}$ may be rewritten as

$$\begin{aligned} |w_{Q_{\mathbf{j},\mathbf{k}}}| &= |\langle x, \varphi_Q \rangle| \\ &\leq \Big(\prod_{i=1}^{N} 2^{j_i/2}\Big) \int |x(\mathbf{t}) - x(\mathbf{0})||\varphi(\mathbf{t} \circ \mathbf{2^j} - \mathbf{k})| \; d\mathbf{t} \\ &\leq c 2^{j./2} \int \|\mathbf{t}\|^{\beta} |\varphi(\mathbf{t} \circ \mathbf{2^j} - \mathbf{k})| \; d\mathbf{t}, \end{aligned}$$

where $\circ$ is simple point-wise or Hadamard product. Note that in previous inequalities, we assumed that the mother wavelet ψ has vanishing moments i.e.

$$\int t_1^{a_1} \dots t_N^{a_N} \varphi(\mathbf{t}) \; d\mathbf{t} = 0,$$

for some $a_1, \dots, a_N \in \mathbb{N}$. By making change of variables $v_i = (t_i 2^{j_i} - k_i)$ in the integration and applying Minkowski inequality, we have

$$\begin{aligned} |w_{Q_{\mathbf{j},\mathbf{k}}}| &\leq c 2^{-j./2} \int \|\mathbf{2^{-j}} \circ (\mathbf{v} + \mathbf{k})\|^{\beta} |\varphi(\mathbf{v})| \; d\mathbf{v} \\ &\leq c 2^{-j./2} \int \|\mathbf{2^{-j}} \circ \mathbf{v}\|^{\beta} \; |\varphi(\mathbf{v})| \; d\mathbf{v} \\ &+ c 2^{-j./2} \|\mathbf{2^{-j}} \circ \mathbf{k}\|^{\beta} \int |\varphi(\mathbf{v})| \; d\mathbf{v}. \end{aligned}$$

Now let $j_{(1)} = \min\{j_1, \dots, j_N\}$. Then the last inequality yields

$$\begin{aligned} |w_{Q_{\mathbf{j},\mathbf{k}}}| &\leq c 2^{-j./2} 2^{-\beta j_{(1)}} \int \|\mathbf{v}\|^{\beta} \; |\varphi(\mathbf{v})| \; d\mathbf{v} \\ &+ c 2^{-j./2} 2^{-\beta j_{(1)}} \|\mathbf{k}\|^{\beta} \int |\varphi(\mathbf{v})| \; d\mathbf{v}. \end{aligned}$$

It seems that in high resolutions the results will be more reliable; nevertheless, for index-β fields the Hölder condition may cause some misleadings in the results. Since $\int \|\mathbf{v}\|^{\beta} \; |\varphi(\mathbf{v})| \; d\mathbf{v} < \infty$, the order of $w_{Q_{\mathbf{j},\mathbf{k}}}$ for index-β fields at resolution $\mathbf{j}$ is $2^{-j./2-\beta j_{(1)}}$. Hence, for very high resolutions w' is dominated by u; this means that by increasing the resolution the effect of w is faded by u. The order of noise term in [30] is $n^{-1/2}$ while it is constant here. Thereupon, our estimator is more flexible in constructing precise decisions by using high reolutions. Note that the method of computing the empirical wavelet coefficients is different from the one used by [30]. On the other hand, in low resolutions the variation of w' is controlled by w. It is worth mentioning that in low resolutions the new problem is letting $\mathbf{j}$ to infinity which may cause failure in preparing a large enough $\mathbf{j}$ to hold the convergence true. Thus, a noticeable point is the behavior of convergence. Surprisingly, the order of noise, is not affected by dimension growth of the random field. More precisely, the noise term affects on estimation only via σ^2.

4. NUMERICAL RESULTS

We partition this section into two main parts. To make a visual sense for the behavior of estimation, a simulation study is presented by employing the observations of Gaussian random fields. The second part contains a solution procedure for the practical problem and a discussion about it.

4.1 Simulation study

There is an exact computation of Hausdorff dimension for index-β family of known Hölder index. Therefore, to construct the lower boundary introduced in Section 1, one of the numerical studies is dedicated to this family to study the out range property of the estimator presented by (10). To study the effect of Hölder index we repeat the numerical computations for the fractional Brownian sheet (fBs).

Using the circulant embedding method, realizations of the 2-dimensional Gaussian field are generated with respect to the stable covariance function:

$$E[X(\mathbf{t})X(\mathbf{0})] = \exp(-c\|\mathbf{t}\|^{\beta}),$$

where $c > 0$ is well-known as topothesy parameter. The fBs is characterized by its variogram that is

$$E|X(\mathbf{t}) - X(\mathbf{0})|^2 = c\|\mathbf{t}\|^{\beta},$$

where c and β are the same as the stable model. The size of each realization is 1024×1024. If x is a realization with respect to this covariance function, then [see 1, Chapter 8]

$$\dim_{\mathrm{H}}(G_x) = 3 - \beta.$$

We add the generated path to a noise matrix constructed by independent standard Gaussian random variables. For $c = 1$, and $\beta = 0.1, 0.3, 0.5, 0.7$ and 0.9, the box dimension estimation is computed based on (10). Furthermore, to obtain the standard deviation, the estimation procedure is replicated 100 times. The results are shown in Table 1. Since there is not another box dimension estimator for multi-dimensional random fields, in addition to the results of our wavelet-based estimator we present the results for five other well-known estimators of Hausdorff dimension. The first two estimators are intrinsic estimators based on line-transect method. In theses methods, the Hurst index is estimated in each row (for horizontal direction) and/or column (for vertical direction) of the gray-scale image data. The final estimate is the median of the results in each direction. The line-transect estimator employs the variation or a variant that uses the second difference (such as oscillation) where the root mean squared errors ($RMSE$) of both are given in Table 1. This table also contains the $RMSE$ of the Hausdorff estimators of Davies and Hall [5], Chan and Wood [3] and Zhu and Stein [31]. All the computations according to the other estimators have been implemented using the `R` package `fractaldim`. The numbers in the parenthesis indicate the number of times which $T(y;\mathbf{j})$ exceeded $\dim_{\mathrm{H}}$.

Table 1. The box dimension estimation and the corresponding standard deviations. The numbers mentioned in parenthesis are the number of out-range estimators

model	β	Wavelet-based		MSE of the other estimators				
		$T(y;(9,9))$	SD	line-transect	second differences	Davies-Hall [5]	Chan-Wood [3]	Zhu-Stein [31]
stable	0.1	2.8719	.04550(5)	.0118	0.0126	.0129	.0118	.0120
	0.3	2.6344	0.04590(7)	.0019	.0030	.0031	.0022	.0024
	0.5	2.4769	0.03874(5)	.0015	.0013	.0015	.0018	.0012
	0.7	2.2828	0.03381(11)	.0654	.0312	.0304	.0799	.0659
	0.9	2.0811	0.03051(13)	.2423	.7315	.0700	.2863	.2425
fBs	0.1	2.9581	0.04959(3)	.0012	.0007	.0010	.0017	.0013
	0.3	2.7200	0.05001(3)	.0013	.0008	.0008	.0013	.0007
	0.5	2.6154	0.04637(6)	.0010	.0013	.0011	.0017	.0007
	0.7	2.4925	0.03696(10)	.0020	.0076	.0081	.0016	.0017
	0.9	2.1645	0.03141(11)	.0024	.0080	.0088	.0020	.0020

The estimator is decreasing in β and therefore increasing in roughness. A simple reason for the growth of standard deviation by reduction of β is the direct relationship between roughness and the fractal dimension. The Hausdorff estimators do not follow this behavior. The $RMSE$ is decreasing when $\beta < 1/2$ and increasing in $\beta > 1/2$. This behavior returns to the change of the dependence structure of index-β family from the short-range to the long-range dependence when the Hölder index crosses $1/2$. Furthermore, due to the restriction of the Hölder index according to the inequality $N \leq \dim_{\mathrm{H}} A (= N + 1 - \beta) \leq \dim_{\mathrm{B}} A$, we expect the greater variance for the estimator of $\dim_{\mathrm{B}}$ in comparison with the variance of the estimators of the Hölder index. Based on the discussion above, the variance of two estimators are not comparable. We are not also able to report the bias of the box dimension estimator since the true parameter is unknown. Moreover, the numeric study shows that the problem of fractal dimension estimation is somehow different from the estimation of the Hölder index. Both the fBs and the stable Gaussian fields have the same Hausdorff dimension for identical β. The $RMSE$ of Hölder index estimators strongly depend on the models, while the features of the box dimension estimation remain constant for both models. This observation demonstrates the main difference between the features of box dimension and Hausdorff dimension estimators. It seems that the box dimension estimation is more appropriate than the Hölder index estimation when the aim of study is measuring the geometrical consequences of the erraticism. On the other hand, even the Hölder index of a fBs is equal with the index of a stable model, the Hölder index estimation does not reflect the same erraticism for theses models.

4.2 Practical problem (continue)

Studying the behavior of particles motion, one may be interested in the self-similarity of the resulting image. Since the path of a particle motion is a fractal, it is expected that this behavior remains in whole paths of particles. Thus, estimating fractal dimension may show the accuracy of this assumption.

Table 2. The means of box dimension estimations for perspective images of solutions at every two minutes

time	mean $T(y;(9,9))$	SD
2	2.7186	0.1698
4	2.6999	0.1868
6	2.7030	0.1515
8	2.6087	0.1486
10	2.5368	0.1357
12	2.4025	0.1311
14	2.3722	0.1289
16	2.4453	0.0784
18	2.1351	0.0342
20	2.0102	0.0071

Simple digital capturing with high resolution and speed, was used to take 96 frames per second of 1024×1024 pictures along 20 minutes. The video capturing has been replicated 30 times and in order to gather the same data, the suspension is well-shaken before each trial. A huge amount of data (3.456×10^6 pictures with 1024×1024 nodes) has been gathered. We need to take $96 \times 60 \times 20 = 115200$ averages of roughness measurements using packages containing 30 pictures. Simply speaking, we have a random sample containing 30 pictures with respect to each frame of digital capturing. In addition to the theoretical restrictions in employing Hausdorff dimension, the cost of computing would be very high. To discover the difficulties of Hausdorff dimension computation for images see [4] and [28]. We employ the fast wavelet transformation to compute surface roughness using the box dimension estimation introduced by (10). The means of the estimated dimensions at every two minutes are provided in Table 2. The suspension becomes more stable by increasing the time and gravity causes the particles to gather in lower levels of the fluid. The pictures which have been taken during the last two minutes are then almost partitioned into a

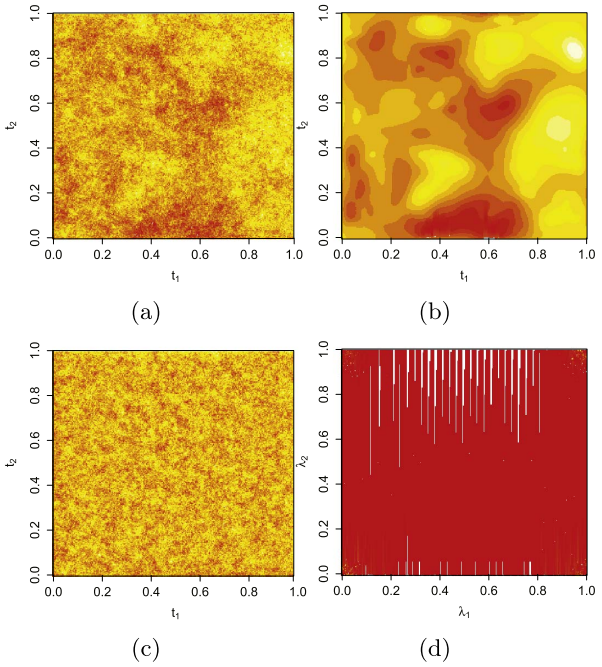

Figure 3. The rescaled captured image (x) when exactly $60s$ passed from the beginning of the experiment (a) and its VisuShrink wavelet estimate (b) or $\hat{x}$; The corresponding residual $r = x - \hat{x}$ (c) and its periodogram (d).

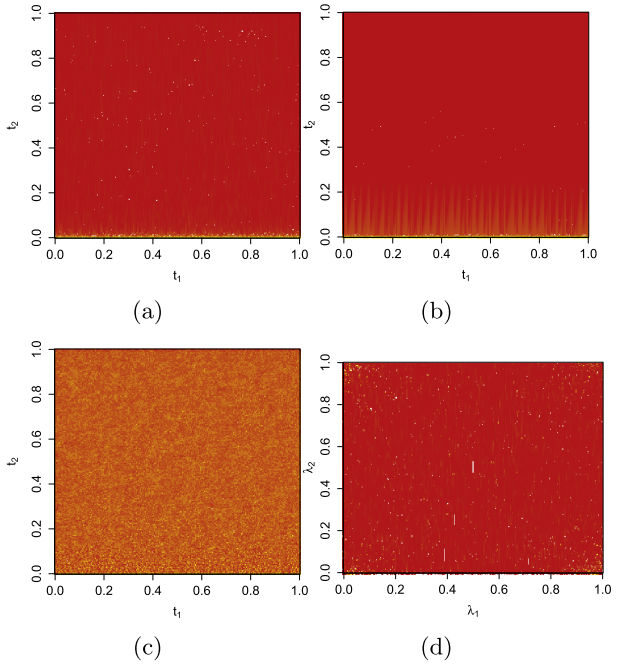

Figure 4. The rescaled captured image (x) when exactly 19 minutes passed from the beginning of the experiment (a) and its VisuShrink wavelet estimate (b) or $\hat{x}$; The corresponding residual $r = x - \hat{x}$ (c) and its periodogram (d).

white rectangle above and a dark one beneath. Thus, they are appeared smooth enough to get an integer dimension. The results show that the dimension of the pictures tend to 2 when we are patient enough. Although the linear pattern is well-fitted between time and dimension, theoretically, better results have been expected from logarithmic curve fitting. One may obtain this claim by means of the box dimension definition. For a given small enough diameter δ, the box dimension is a logarithmic function of $\mathcal{C}_\delta$ and cubic polynomial regression strongly determines the relationship between $\mathcal{C}_\delta$ and time.

Concerning the model diagnosis, we only demonstrate the procedure for two specific times of the experiment: 1) the gray-scale image generated after 60 seconds; 2) the gray-scale image generated after 19 minutes from the beginning of the experiment. Figures 3(a) and 4(a) demonstrate two observed gray-scale perspective images after one and 19 minutes from shaking the suspension, respectively. Only for better demonstration we show the pictures in 256×256 resolution while the original images are constructed by 1024×1024 pixels. Noe that the images are rescaled and so the areas of the yellow parts (which estimate the volume of particles) are not equal in 3(a) and 4(a). However, Figure 4(a) shows the equilibration or sedimentation in the floor of the container. Daubechies wavelet with three vanishing moments is used for estimating x (Figures 3(b) and 4(b)) and the corresponding residuals are shown in Figures 3(c) and 4(c). Figures 3(d) and 4(d) show the periodograms of the residuals and we have identical values of periodograms for almost all the frequencies particularly when $\boldsymbol{\lambda}$ is far enough from the edges of the window. In fact, the small frequency-varying behavior in these figures are due to the edge effect in applying the fast Fourier transform during the computation of the periodogram.

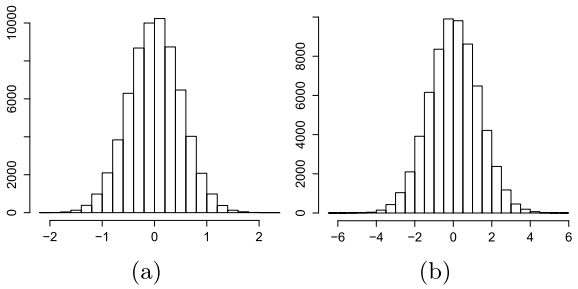

Figure 5. The histograms of residuals after 60 seconds (a) and after 19 minutes (b) from the beginning of the experiment.

Figures 5(a) and 5(b) represents the histograms of the residuals detected in previous figures. The histograms visually verify the normality assumption that is also accepted using the Kolomogorov-Smirnov test. The p-values of the normality test of the residuals of the images captured after 60 seconds and 19 minutes are respectively 0.9101 and 0.5156. The positive small skewness of the Figure 5(a) makes us cu-

rious to replace the normality assumption with the skewed-normality in the null hypothesis of the Kolmogorov-Smirnov test. Again the null hypothesis of the skewed-normality is not rejected for both the residuals with p-values equal to 0.5848 and 0.8743, respectively. As mentioned at the beginning of Section 3.2, this uncertainty between the normality and the skewed-normality only make us suspicious about the minimaxity of the universal threshold λ_{n^*}.

5. DISCUSSION

One may denoise the surface before performing any estimation procedure to ensure that the estimated parameter of roughness measurement is specialized to the surface and is not affected by noise. An efficient method of denoising is based on the wavelet approximation. Projecting the surface onto spaces generated by mother and father wavelets, this method decomposes the surface into two approximation and detail parts, respectively. Since the surface is observed on discrete nodes of the lattice, the projection is strongly affected by the width of the windows which used for estimating the approximation coefficients with respect to mother wavelet. Just like our method, the problem of resolution is arisen here again. In low resolutions, we may loose some parts of the surface and in high resolutions the approximated surface is not well-denoised. According to the wavelet shrinkage technique, denoising is succeeded optimally. After denoising, we will confront the difficulties of using intrinsic estimators discussed in Section 1. Therefore, if denoising is based on wavelet methods, it can be seen an equivalence between this approach and the one introduced in this paper.

APPENDIX A. PROOF OF THEOREM 3.1

The technique of the proof is similar to one mentioned by Wang [30]. According to the definition of soft threshold, we have

$$\begin{aligned}\sum_{\mathbf{k}} \sup_{Q_{\mathbf{j}',\mathbf{k}'}} |w'_{Q_{\mathbf{j_n},\mathbf{k}}}| - 2^{j.\mathbf{n}}\lambda_{n_*} &\leq \sum_{\mathbf{k}} |\sup_{Q_{\mathbf{j}',\mathbf{k}'}} \eta_S(w'_{Q_{\mathbf{j_n},\mathbf{k}}})| \\ &\leq \sum_{\mathbf{k}} \sup_{Q_{\mathbf{j}',\mathbf{k}'}} |w'_{Q_{\mathbf{j_n},\mathbf{k}}}|. \qquad (11)\end{aligned}$$

Since ε is a white noise, u_Q is a white noise as well and hence $\sum_{\mathbf{k}} |u_{Q_{\mathbf{j_n},\mathbf{k}}}| = O_p(2^{j.\mathbf{n}})$. Thus, by equation (9) in one hand we have

$$\begin{aligned}&\log_2\left(\sum_{\mathbf{k}} \sup_{Q_{\mathbf{j}'_\mathbf{n},\mathbf{k}'}} |w'_{Q_{\mathbf{j}'_\mathbf{n},\mathbf{k}'}}|\right) \\ &\leq \log_2\left(\sum_{\mathbf{k}} \sup_{Q_{\mathbf{j}'_\mathbf{n},\mathbf{k}'}} |w_{Q_{\mathbf{j}'_\mathbf{n},\mathbf{k}'}}| + n_*^{-1/2}\sum_{\mathbf{k}} \sup_{Q_{\mathbf{j}'_\mathbf{n},\mathbf{k}'}} |u_{Q_{\mathbf{j}'_\mathbf{n},\mathbf{k}'}}|\right) \\ &= \log_2\left(\sum_{\mathbf{k}} \sup_{Q_{\mathbf{j}'_n,\mathbf{k}'}} |w_{Q_{\mathbf{j}'_n,\mathbf{k}'}}| + O_p(n_*^{-1/2}2^{j.\mathbf{n}})\right) \\ &= \log_2\left(\sum_{\mathbf{k}} \sup_{Q_{\mathbf{j}'_\mathbf{n},\mathbf{k}'}} |w_{Q_{\mathbf{j}'_\mathbf{n},\mathbf{k}'}}|\right) \\ &+ \log_2\left(1 + O_p\Big(\frac{n_*^{-1/2}2^{j.\mathbf{n}}}{\sum \sup |w|}\Big)\right) \\ &= \log_2\left(\sum_{\mathbf{k}} \sup_{Q_{\mathbf{j}'_\mathbf{n},\mathbf{k}'}} |w_{Q_{\mathbf{j}'_\mathbf{n},\mathbf{k}'}}|\right) + O_p\Big(\frac{n_*^{-1/2}2^{j.\mathbf{n}}}{\sum \sup |w|}\Big). \qquad (12)\end{aligned}$$

On the other hand,

$$\begin{aligned}&\log_2\left(\sum_{\mathbf{k}} \sup_{Q_{\mathbf{j}'_\mathbf{n},\mathbf{k}'}} |w'_{Q_{\mathbf{j}'_\mathbf{n},\mathbf{k}'}}| - 2^{j.\mathbf{n}}\lambda_{n_*}\right) \\ &\leq \log_2\left(\sum_{\mathbf{k}} \sup_{Q_{\mathbf{j}'_\mathbf{n},\mathbf{k}'}} |w_{Q_{\mathbf{j}'_\mathbf{n},\mathbf{k}'}}| + O_p(n_*^{-1/2}2^{j.\mathbf{n}}) - 2^{j.\mathbf{n}}\lambda_{n_*}\right) \\ &= \log_2\left(\sum_{\mathbf{k}} \sup_{Q_{\mathbf{j}'_\mathbf{n},\mathbf{k}'}} |w_{Q_{\mathbf{j}'_\mathbf{n},\mathbf{k}'}}|\right) \\ &+ \log_2\left(1 + \frac{O_p(n_*^{-1/2}2^{j.\mathbf{n}}) - 2^{j.\mathbf{n}}\lambda_{n_*}}{\sum \sup |w|}\right) \\ &= \log_2\left(\sum_{\mathbf{k}} \sup_{Q_{\mathbf{j}'_\mathbf{n},\mathbf{k}'}} |w_{Q_{\mathbf{j}'_\mathbf{n},\mathbf{k}'}}|\right) \\ &+ O_p\left(\frac{2^{j.\mathbf{n}}(n_*^{-1/2} - \lambda_{n_*})}{\sum \sup |w|}\right) \\ &= \log_2\left(\sum_{\mathbf{k}} \sup_{Q_{\mathbf{j}'_\mathbf{n},\mathbf{k}'}} |w_{Q_{\mathbf{j}'_\mathbf{n},\mathbf{k}'}}|\right) \\ &+ O_p\left(\frac{2^{j.\mathbf{n}}n_*^{-1/2}\sqrt{\log n_*})}{\sum \sup |w|}\right) \qquad (13)\end{aligned}$$

To remove the stochastic order part, according to (6) we obtain

$$\frac{2^{j.\mathbf{n}}(\log n_*)^{1/2}}{\sum \sup |w|} = 2^{(2-\overline{\dim}_{\mathrm{B}}G_x)j.\mathbf{n}}\frac{\sqrt{\log n_*}}{j.\mathbf{n}} \to 0, \qquad (14)$$

as $\mathbf{j_n} \to \boldsymbol{\infty}$ without any further assumption on $j.\mathbf{n}$

Applying (14) onto (13) and employing (13), we achieve

$$\begin{aligned}\frac{\log_2\left(\sum_{\mathbf{k}} \sup_{Q_{\mathbf{j}'_\mathbf{n},\mathbf{k}'}} |w'_{Q_{\mathbf{j}'_\mathbf{n},\mathbf{k}'}}|\right)}{j.\mathbf{n}} &\xrightarrow{p} \overline{\dim}_{\mathrm{B}}G_x - 1, \\ \frac{\log_2\left(\sum_{\mathbf{k}} \sup_{Q_{\mathbf{j}'_\mathbf{n},\mathbf{k}'}} |w'_{Q_{\mathbf{j}'_\mathbf{n},\mathbf{k}'}}| - 2^{j.\mathbf{n}}\lambda\right)}{j.\mathbf{n}} &\xrightarrow{p} \overline{\dim}_{\mathrm{B}}G_x - 1,\end{aligned}$$

where using (11) completes the proof.

Received 11 March 2015

REFERENCES

[1] Adler, R. J. (1981). *The geometry of random fields*. Wiley, Chichester. MR611857

[2] Barnsley, M. (1988). *Fractals everywhere*. Academic Press, Boston. MR977274

[3] Chan, G. and Wood, A. T. A. (2000). Increment-based estimators of fractal dimension for two-dimensional surface data. *Statist. Sinica* **10** 343–376. MR1769748

[4] Chan, G. and Wood, A. T. A. (2004). Estimation of fractal dimension for a class of non-Gaussian stationary processes and fields. *Ann. Statist.* **32** 1222–1260. MR2065204

[5] Davies, S. and Hall, P. (1999). Fractal analysis of surface roughness by using spatial data. *J. R. Stat. Soc. Ser. B Stat. Methodol.* **61** 3–37. MR1664088

[6] Deliu, A. and Jawerth, B. (1992). Geometrical dimension versus smoothness. *Constr. Approx.* **8** 211–222. MR1152878

[7] Donoho, D. L. and Johnstone, I. M. (1994). Ideal spatial adaptation by wavelet shrinkage. *Biometrika* **81** 425–455. MR1311089

[8] Donoho, D. L. and Johnstone, I. M. (1995). Adapting to unknown smoothness via wavelet shrinkage. *J. Amer. Statist. Assoc.* **90** 1200–1224. MR1379464

[9] Einstein, A. (1905). On the motion of small particles suspended in liquids at rest required by the molecular-kinetic theory of heat (in German). *Ann. Phys.* **17** 549–560.

[10] Gneiting, T., Ševčíková, H. and Percival, D. B. (2012). Estimators of fractal dimension: assessing the roughness of time series and spatial data. *Statist. Sci.* **27** 247–277. MR2963995

[11] Hall, P. and Wood, A. (1993). On the performance of box-counting estimators of fractal dimension. *Biometrika* **80** 246–252. MR1225230

[12] Hunt, B. R. (1996). Maximum local Lyapunov dimension bounds the box dimension of chaotic attractors. *Nonlinearity* **9** 845–852. MR1399474

[13] Hunt, F. (1990). Error analysis and convergence of capacity dimension algorithms. *SIAM J. Appl. Math.* **50** 307–321. MR1036244

[14] Hunt, F. and Sullivan, F. (1989). Methods of computing fractal dimensions. In *Nonlinear semigroups, partial differential equations and attractors (Washington, DC, 1987)* 83–95. Springer, Berlin. MR1021016

[15] Jaffard, S. (1998). Oscillation spaces: properties and applications to fractal and multifractal functions. *J. Math. Phys.* **39** 4129–4141. MR1633152

[16] Kamont, A. and Wolnik, B. (1999). Wavelet expansions and fractal dimensions. *Constr. Approx.* **15** 97–108. MR1660073

[17] Mallat, S. (1989). A theory for multiresolution signal decomposition: the wavelet representation. *IEEE Trans. on Pattern Anal. Mach. Intell.* **11** 674–693.

[18] Mandelbrot, B. B. (1967). How long is the coast of Britain. *Science* **156** 636–638.

[19] Marinucci, D. (2004). Testing for non-Gaussianity on cosmic microwave background radiation: a review. *Statist. Sci.* **19** 294–307. MR2140543

[20] Massopust, P. R. (1994). *Fractal functions, fractal surfaces, and wavelets*. Academic Press, San Diego. MR1313502

[21] Misiti, M., Misiti, Y., Oppenheim, G. and Poggi, J.-M. (2007). *Wavelets and their applications*. ISTE, London. MR2447159

[22] Ogata, Y. and Katsura, K. (1991). Maximum likelihood estimates of the fractal dimension for random spatial patterns. *Biometrika* **78** 463–474. MR1130915

[23] Pagano, M. (1971). Some asymptotic properties of a two-dimensional periodogram. *J. Appl. Probability* **8** 841–847. MR0292247

[24] Peitgen, H. O., Jürgens, H. and Saupe, D. (2004). *Chaos and fractals – new frontiers of science*. 2nd edn. Springer, New York. MR2031217

[25] Richardson, L. F. (1961). The problem of contiguity: an appendix of statistics of deadly quarrels. *Gen. Sys. Year B.* **6** 139–187.

[26] Sullivan, F. and Hunt, F. (1988). How to estimate capacity dimension. *Nucl. Phys. B Proc. Suppl.* **5A** 125–128.

[27] Taheriyoun, A. R. (2012). Testing the covariance function of stationary Gaussian random fields. *Statist. Probab. Lett.* **82** 606–613. MR2887478

[28] Taheriyoun, A. R. and Shafie, K. (Unpublished results). Estimation of fractal dimension of Gaussian fields via Euler characteristic.

[29] Taylor, C. C. and Taylor, S. J. (1991). Estimating the dimension of a fractal. *J. Roy. Statist. Soc. Ser. B* **53** 353–364. MR1108332

[30] Wang, Y. (1997). Fractal function estimation via wavelet shrinkage. *J. Roy. Statist. Soc. Ser. B* **59** 603–613. MR1452028

[31] Zhu, Z. and Stein, M. L. (2002). Parameter estimation for fractional Brownian surfaces. *Statist. Sinica* **12** 863–883. MR1929968

Ali Reza Taheriyoun
Department of Statistics
Shahid Beheshti University
Evin, 1983969411
Tehran
Iran
E-mail address: a_taheriyoun@sbu.ac.ir

Yazhen Wang
Department of Statistics
University of Wisconsin
Medical Science Center
1300 University Avenue
Madison, WI53706
USA
E-mail address: yzwang@stat.wisc.edu